Mechanism and Machine Theory 50 (2012) 134–149

Contents lists available at SciVerse ScienceDirect

Mechanism and Machine Theory

journal homepage: www.elsevier.com/locate/mechmt

Nonlinear vibration control of a cantilever beam by a nonlinear energy sink

Z. Nili Ahmadabadi [b], S.E. Khadem [a,b,*]

[a] Khadem Mechanical Engineering Research Center, P.O. Box 14115-177, Tehran, Iran
[b] Department of Aerospace and Mechanical Engineering, Tarbiat Modares University, P.O. Box 14115-177, Tehran, Iran

ARTICLE INFO

Article history:
Received 5 February 2011
received in revised form 29 August 2011
accepted 9 November 2011
Available online 15 December 2011

Keywords:
Nonlinear energy sink
Nonlinear normal mode
Nonlinear energy pumping
Nonlinear vibration control
Beam

ABSTRACT

This paper investigates the effect of an attached/coupled nonlinear energy sink (NES[1]) on energy suppression of a cantilever beam under shock excitation. Grounded and ungrounded configurations of NES are studied and the NES performance is optimized through variation of different parameters. The realization of nonlinear vibration control through one-way irreversible nonlinear energy pumping and optimizing the system parameters result in acquiring up to 89% dissipation of the ungrounded system energy imposed by shock excitation. In addition, the bifurcations and topological structure of nonlinear normal modes (NNMs[2]) of both systems are studied in order to find necessary conditions of targeted energy transfer (TET[3]) realization in each configuration. In fact, the role of NNMs in identifying dynamics of energy pumping in especially continuous systems is studied for the first time.

1. Introduction

A great attention has been recently paid to employing NES as an essential nonlinear energy absorber rather than linear absorbers or weakly nonlinear absorbers.

Applications of the NES in 2-DOF or multi-DOF systems of weakly coupled linear and essentially nonlinear damped oscillators with different parameters and conditions were studied widely for nonlinear energy pumping and a variety of system response regimes in [1–5]. 2DOF systems comprised of a linear oscillator and an attached NES with pure cubic nonlinearity were considered in [6–13], as well. Moreover, in studies [14–15], application of the NES in attenuating the self-excited oscillations of a van der Pol oscillator, and also different response regimes were examined. On the other hand, dissipated energy by an attached NES to a simply supported beam was examined in [16].

The importance of the topological structure of NNMs of a non-dissipative and unforced system in TET of a dissipative system was studied for a multi-DOF system of linear oscillators coupled to a NES in [17]. Indeed, it was proven that dynamics of energy pumping mainly relied on the structure of these modes for discrete systems.

In this work, for the first time a linear continuous system (a finite length beam) with two different NES configurations (grounded and ungrounded) will be considered for optimizing the amount of energy dissipation. Then, the conditions of TET realization in each system will be introduced through evaluation of the NNMs structures. In fact, by comparing the results obtained from dissipated and instantaneous energies of each system with the structure of corresponding NNMs, the important role of NNMs in irreversible energy pumping will be proven for continuous systems.

* Corresponding author. Tel./fax: +98 21 82883388.
E-mail address: khadem@modares.ac.ir (S.E. Khadem).

[1] Nonlinear energy sink.
[2] Nonlinear normal modes.
[3] Targeted energy transfer.

0094-114X/$ – see front matter © 2011 Elsevier Ltd. All rights reserved.
doi:10.1016/j.mechmachtheory.2011.11.007

2. Model analysis

Consider a cantilever beam which is attached to an NES and is under shock excitation. Nonlinear attachment is examined in two different configurations as shown in Fig. 1: grounded and ungrounded. In the grounded configuration, the NES is weakly coupled to the beam.

Applying Euler–Bernoulli beam theory, the equations of motion for two configurations would be in the following forms:

Grounded configuration, NES#1,

$$\begin{aligned} &EIy_{xxxx}(x,t)+My_{tt}(x,t)+\varepsilon\beta y_t(x,t)+\varepsilon k_1[y(d,t)-w(t)]\delta(x-d)=F(t)\delta(x-s)\\ &\varepsilon M\ddot{w}(t)+\varepsilon k_1[w(t)-y(d,t)]+kw^3(t)+\varepsilon C\dot{w}(t)=0 \end{aligned} \tag{1}$$

Ungrounded configuration, NES#2,

$$\begin{aligned} &EIy_{xxxx}(x,t)+My_{tt}(x,t)+\varepsilon\beta y_t(x,t)+\left\{\varepsilon k[y(d,t)-w(t)]^3+\varepsilon C[y_t(d,t)-\dot{w}(t)]\right\}\delta(x-d)=F(t)\delta(x-s)\\ &\varepsilon M\ddot{w}(t)+\varepsilon k[w(t)-y(d,t)]^3+\varepsilon C[\dot{w}(t)-y_t(d,t)]=0 \end{aligned} \tag{2}$$

where dot denotes the differentiation with respect to t, and subscript x or t shows partial differentiation; E and EI are the Young's modulus and bending stiffness of the beam, respectively; M is the beam mass; k_1 and k are the coupling spring stiffness and the spring stiffness of the NES; β and C are the damping coefficients; $\delta(x-d)$ is the Dirac function; s and d are the place of applying the external load and attaching the NES, respectively; $\varepsilon \ll 1$. It should be mentioned that since the comparison between NES#1 and NES#3, shown in Fig. 1c, is not possible (because the NES is free of load and does not play any role in this system), the comparison will be made between NES#1 and NES#2.

The nth vibration mode Φ_n and frequency ω_n of a cantilever beam are,

$$\begin{aligned} &\Phi_n(x)=A_n\{[\sin(\beta_nL)-\sinh(\beta_nL)][(\sin(\beta_nx)-\sinh(\beta_nx))]+[\cos(\beta_nL)+\cosh(\beta_nL)][(\cos(\beta_nx)-\cosh(\beta_nx))]\}\\ &\omega_n=\beta_n^2\sqrt{\frac{EI}{M}}\\ &A_n=\left\{\int_{x=0}^{L}M\left[\frac{\Phi_n(x)}{A_n}\right]^2dx\right\}^{\frac{-1}{2}} \end{aligned} \tag{3}$$

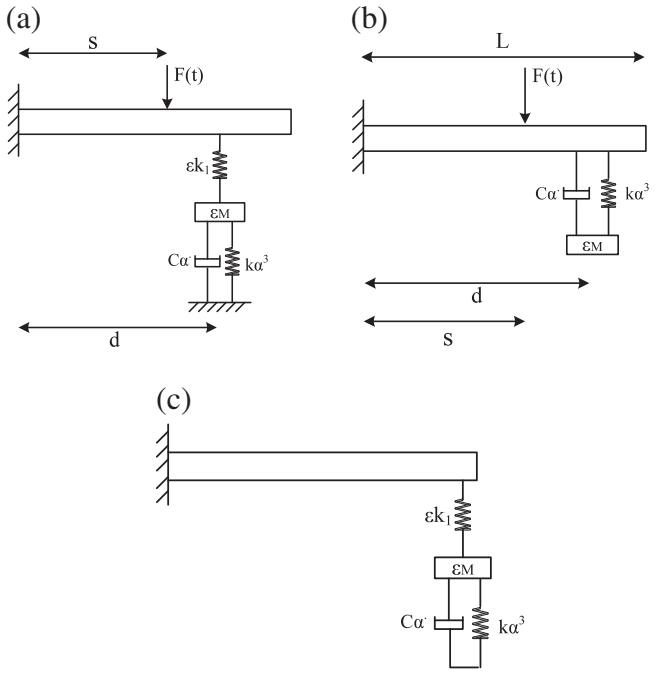

Fig. 1. NES configurations: (a) configuration of NES#1, (b) configuration of NES#2, (c) configuration of NES#3.

where A_n and L are amplitude and length of the beam. β_n will be obtained by solving the following equation:

$$\cos(\beta_n L)\cosh(\beta_n L) = -1$$

In order to express Eqs. (1) and (2) in non-dimensional form, the non-dimensional variables are defined as

$$\bar{x} = \frac{x}{L}, \bar{y} = \frac{y}{L}, \bar{w} = \frac{w}{L}, \tau = \frac{t}{L^2}\sqrt{\frac{EI}{M}}, \bar{k} = \frac{kL^6}{EI}, \bar{\beta} = \beta\frac{L^2}{\sqrt{EIM}}, \bar{C} = C\frac{L^2}{\sqrt{EIM}}, \bar{F}(\tau) = F(t)\frac{L^3}{EI}, \bar{k}_1 = k_1\frac{L^4}{EI}.$$

By introducing the non-dimensional variables into the system of Eqs. (1) and (2), they will be reduced to the following dimensionless form:

NES#1,

$$\begin{aligned} &\bar{y}_{\bar{x}\bar{x}\bar{x}\bar{x}}(\bar{x},\tau) + \bar{y}_{\tau\tau}(\bar{x},\tau) + \varepsilon\bar{\beta}\bar{y}_{\tau}(\bar{x},\tau) + \varepsilon\bar{k}_1\left[\bar{y}\left(\frac{d}{L},\tau\right) - \bar{w}(\tau)\right]\delta\left(\bar{x} - \frac{d}{L}\right) = \bar{F}(\tau)\delta\left(\bar{x} - \frac{s}{L}\right) \\ &\varepsilon\ddot{\bar{w}}(\tau) + \varepsilon\bar{k}_1\left[\bar{w}(\tau) - \bar{y}\left(\frac{d}{L},\tau\right)\right] + \bar{k}\bar{w}^3(\tau) + \varepsilon\bar{C}\dot{\bar{w}}(\tau) = 0 \end{aligned} \tag{4}$$

NES#2,

$$\begin{aligned} &\bar{y}_{\bar{x}\bar{x}\bar{x}\bar{x}}(\bar{x},\tau) + \bar{y}_{\tau\tau}(\bar{x},\tau) + \varepsilon\bar{\beta}\bar{y}_{\tau}(\bar{x},\tau) + \left\{\varepsilon\bar{k}\left[\bar{y}\left(\frac{d}{L},\tau\right) - \bar{w}(\tau)\right]^3 + \varepsilon\bar{C}\left[\bar{y}_{\tau}\left(\frac{d}{L},\tau\right) - \dot{\bar{w}}(\tau)\right]\right\}\delta\left(\bar{x} - \frac{d}{L}\right) = \bar{F}(\tau)\delta\left(\bar{x} - \frac{s}{L}\right) \\ &\varepsilon\ddot{\bar{w}}(\tau) + \varepsilon\bar{k}\left[\bar{w}(\tau) - \bar{y}\left(\frac{d}{L},\tau\right)\right]^3 + \varepsilon\bar{C}\left[\dot{\bar{w}}(\tau) - \bar{y}_{\tau}\left(\frac{d}{L},\tau\right)\right] = 0 \end{aligned} \tag{5}$$

Galerkin method is used in order to acquire the equations of motion in an infinite set of ordinary differential equations. So, the displacement can be thus expressed as:

$$\bar{y}(\bar{x},\tau) = \sum_{n=0}^{\infty} q_n(\tau)\Phi_n(\bar{x}). \tag{6}$$

Now, using orthogonality condition, one obtains:

NES#1,

$$\begin{aligned} &b_{fh}\ddot{q}_h(\tau) + \varepsilon\bar{\beta}b_{fh}\dot{q}_h(\tau) + b_{sh}q_h(\tau) + \varepsilon\bar{k}_1\left[\sum_{r=0}^{\infty} q_r(\tau)\Phi_r\left(\frac{d}{L}\right) - \bar{w}(\tau)\right]\Phi_h\left(\frac{d}{L}\right) = \bar{F}(\tau)\Phi_h\left(\frac{s}{L}\right), \quad h = 0,\ldots,\infty \\ &\varepsilon\ddot{\bar{w}}(\tau) + \varepsilon\bar{k}_1\left[\bar{w}(\tau) - \sum_{r=0}^{\infty} q_r(\tau)\Phi_r\left(\frac{d}{L}\right)\right] + \bar{k}\bar{w}^3(\tau) + \varepsilon\bar{C}\dot{\bar{w}}(\tau) = 0 \end{aligned} \tag{7}$$

NES#2,

$$\begin{aligned} &b_{fh}\ddot{q}_h(\tau) + \varepsilon\bar{\beta}b_{fh}\dot{q}_h(\tau) + b_{sh}q_h(\tau) + \left\{\varepsilon\bar{k}\left[\sum_{r=0}^{\infty} q_r(\tau)\Phi_r\left(\frac{d}{L}\right) - \bar{w}(\tau)\right]^3 + \varepsilon\bar{C}\left[\sum_{r=0}^{\infty}\dot{q}_r(\tau)\Phi_r\left(\frac{d}{L}\right) - \dot{\bar{w}}(\tau)\right]\right\}\Phi_h\left(\frac{d}{L}\right) = \\ &\bar{F}(\tau)\Phi_h\left(\frac{s}{L}\right), \quad h = 0,\ldots,\infty \\ &\varepsilon\ddot{\bar{w}}(\tau) + \varepsilon\bar{k}\left[\bar{w}(\tau) - \sum_{r=0}^{\infty} q_r(\tau)\Phi_r\left(\frac{d}{L}\right)\right]^3 + \varepsilon\bar{C}\left[\dot{\bar{w}}(t) - \sum_{r=0}^{\infty}\dot{q}_r(\tau)\Phi_r\left(\frac{d}{L}\right)\right] = 0 \end{aligned} \tag{8}$$

where:

$$b_{fh} = \int_{\bar{x}=0}^{1}\Phi_h^2(\bar{x})d\bar{x}$$
$$b_{sh} = \int_{\bar{x}=0}^{1}\frac{d^4\Phi_h(\bar{x})}{d\bar{x}^4}\Phi_h(\bar{x})d\bar{x}$$

Values of b_{fh}, b_{sh}, Φ, and βL for each mode are shown in Table 1.
The external shock load applied at $\bar{x} = 1$, would be in the following form:

$$F(t) = BHeaviside\left(\frac{T}{2} - t\right)\sin\left(\frac{2\pi t}{T}\right)$$

Table 1
Corresponding values of b_{fh}, b_{sh}, Φ,and βL for each mode.

Mode number	βL	Φ	b_f	b_s
0	3.5160	−2.00	0.999	12.362
1	22.0345	2.00	1.00	485.519
2	61.6972	−2.00	1.00	3806.546
3	120.9019	2.067	1	14,617.27
4	199.8595	−0.45	1	39,943.83

The portion of the external load energy dissipated through the NES damper can be obtained using the following relation:

NES#1,

$$P(\tau)\equiv\frac{\int_0^{\tau}\varepsilon\bar{C}\dot{w}(z)^{\alpha}dz}{\int_0^{T}\bar{F}(\tau)\sum_{n=0}^{\infty}\dot{q}_n(\tau)\Phi_n\left(\frac{s}{L}\right)d\tau} \tag{9}$$

NES#2,

$$P(\tau)\equiv\frac{\int_0^{\tau}\varepsilon\bar{C}\left\{\left[\dot{w}(z)-\sum_{n=0}^{\infty}\dot{q}_n(z)\Phi_n\left(\frac{d}{L}\right)\right]\right\}^{\alpha}dz}{\int_0^{T}\bar{F}(\tau)\sum_{n=0}^{\infty}\dot{q}_n(\tau)\Phi_n\left(\frac{s}{L}\right)d\tau}.$$

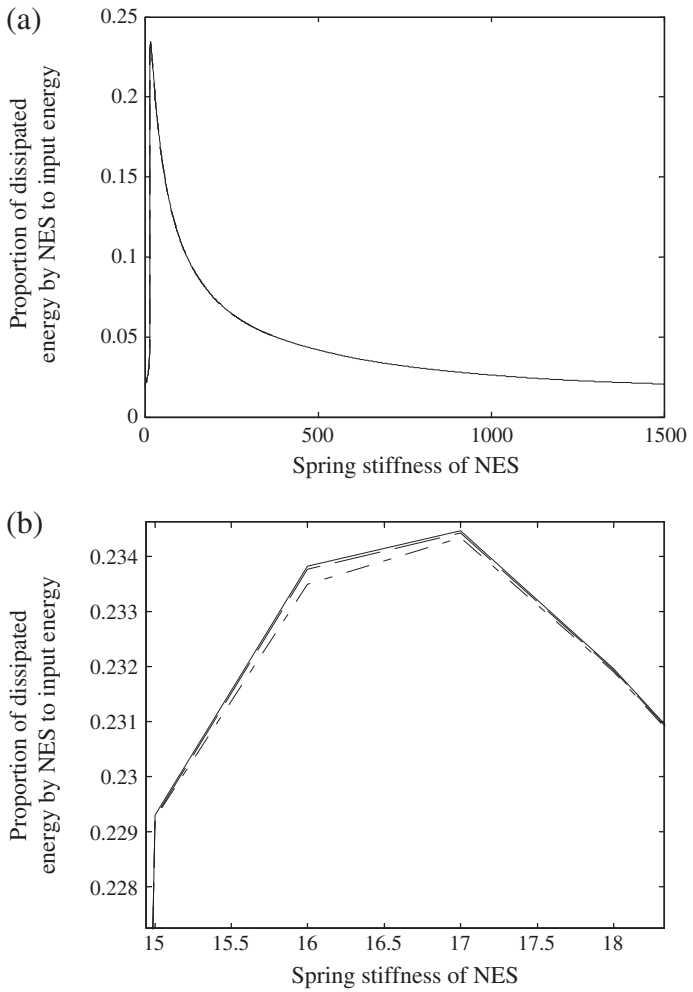

Fig. 2. NES#1: (a) input energy dissipated by the NES as a function of the NES spring stiffness for a shortened system with 2, 5 and 6 modes, and (b) close-up. Dash-dot line: 2 modes; solid line: 5 modes, dash line: 6 modes.

In case of linear damper, α would be equal to 2.

In order to compute the transient dynamics of NES#1 and 2, the numerical integration of Eqs. (7) and (8) should be performed by considering a finite number of modes. Therefore, the results of the numerical integrations for shortened systems with different number of modes are examined. The results are plotted in Figs. 2 and 3. According to these plots, there is no significant difference between the results obtained by considering 5 modes and 6 modes. So evidently, the required accuracy for computing the transient dynamics of the systems is attained by considering the first 5 modes. Consequently, just these modes are taken into account for all forthcoming computations.

The next step would be tuning the NES parameters (i.e. ε, the NES position, the NES damping coefficient and spring stiffness) for optimization of the NES performance in both configurations. For some reasons which will become clear in the next sections, the optimization of the NES performance of NES#1 is more discussed, and just the corresponding results of the optimization of NES#2 will be presented.

The NES position (d) is one of the parameters which need to be tuned. According to Fig. 5, the maximum energy dissipation in NES#1 occurs when the NES is attached to the free end of the beam. This is also true for NES#2, but for the sake of brevity, the corresponding figure is not shown here. So, the NES will be attached to the beam at $\bar{x} = 1$ in both configurations in further analysis.

Figs. 2–4 show strong dependence of the energy dissipation percentage on the spring stiffness of the NES for both mentioned configurations and on parameter $\bar{B}$ for NES#1. It may be noted that there is a significant difference between the amounts of dissipated energy in these configurations, e.g. maximum energy dissipation in NES#2 is 89% of input energy which takes place at $\bar{k} = 13$, whereas this amount drops to only about 23% of input energy in NES#1 at $\bar{k} = 17$.

But there are still other two parameters (ε and the NES damping coefficient) which might effect on the NES optimization. Fig. 6 depicts contour plots of input energy dissipated by NES as a function of each pair of the NES parameters for NES#1. Varying the

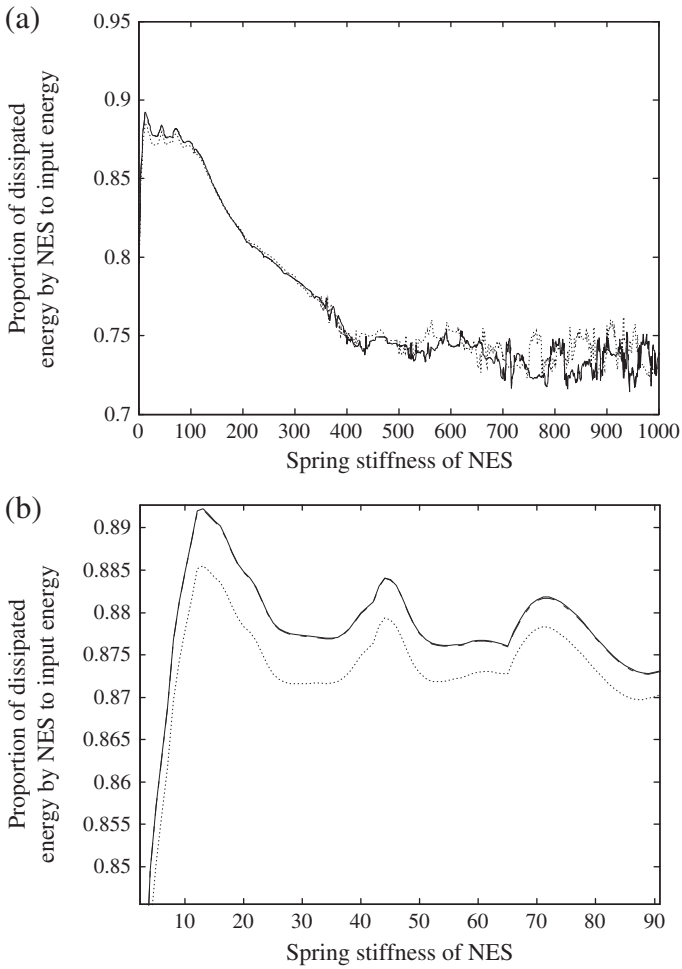

Fig. 3. NES#2: (a) input energy dissipated by the NES as a function of the NES spring stiffness for a shortened system with 2, 5 and 6 modes, and (b) close-up. Dash line: 2 modes; solid line: 5 modes, dash-dot line: 6 modes.

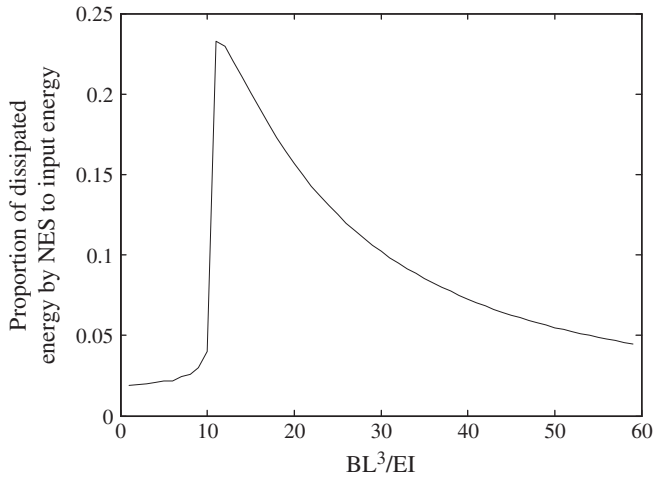

Fig. 4. Input energy dissipated by NES#1 as a function of load amplitude $\bar{B} = B\frac{L^3}{EI}$.

NES parameters over a broad range and observing the effects of these changes on dissipated energy by the NES, reveal the fact that the maximum energy dissipation in NES#1 does not increase to more than 23%.

In studying the NNMs of this system (next section), it will be demonstrated that the influential parameters on TET of the system are just ε, the NES position and spring stiffness. So, just optimizing these parameters is sufficient for comparing energy pumping in two configurations.

The optimal parameters are shown in Table 2 and will be used in further analysis.

Studying instantaneous energy in the NES of each configuration might be helpful in obtaining more details about this occurrence.

Fig. 11 shows the existence of 1:1 resonance capture in the system and that the motion is strongly localized to the NES. Furthermore, Fig. 12 shows nonlinear beating in the initial time which will lead to an irreversible energy pumping afterward. Indeed, TET realization is the main reason for the high energy dissipation in NES#2. On the other hand, the motion localizes to the beam for NES#1, and there is no remarkable energy pumping for any values of parameter $\bar{B}$ (see Figs. 7–10).

The parameter values are employed according to Table 2.

3. Nonlinear normal modes

3.1. NES#2

The NNMs of the non-dissipative system are considered as crucial factors in TET of the dissipative system, and so, the investigation of these modes bifurcations and structures will help to recognize the conditions for TET realization. In this section, the

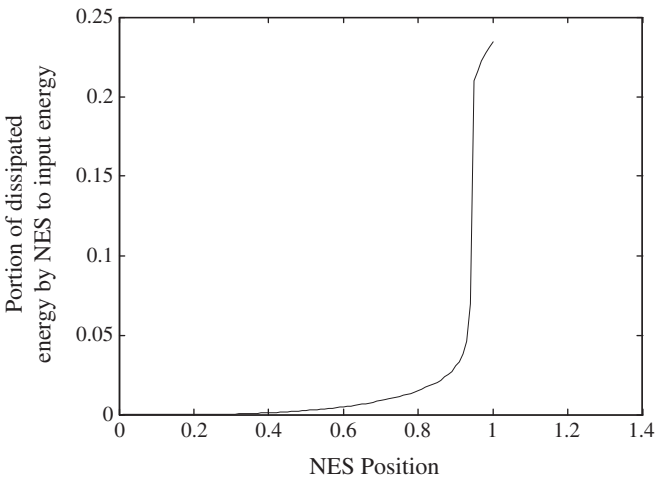

Fig. 5. Input energy dissipated by NES#1 as a function of the NES position.

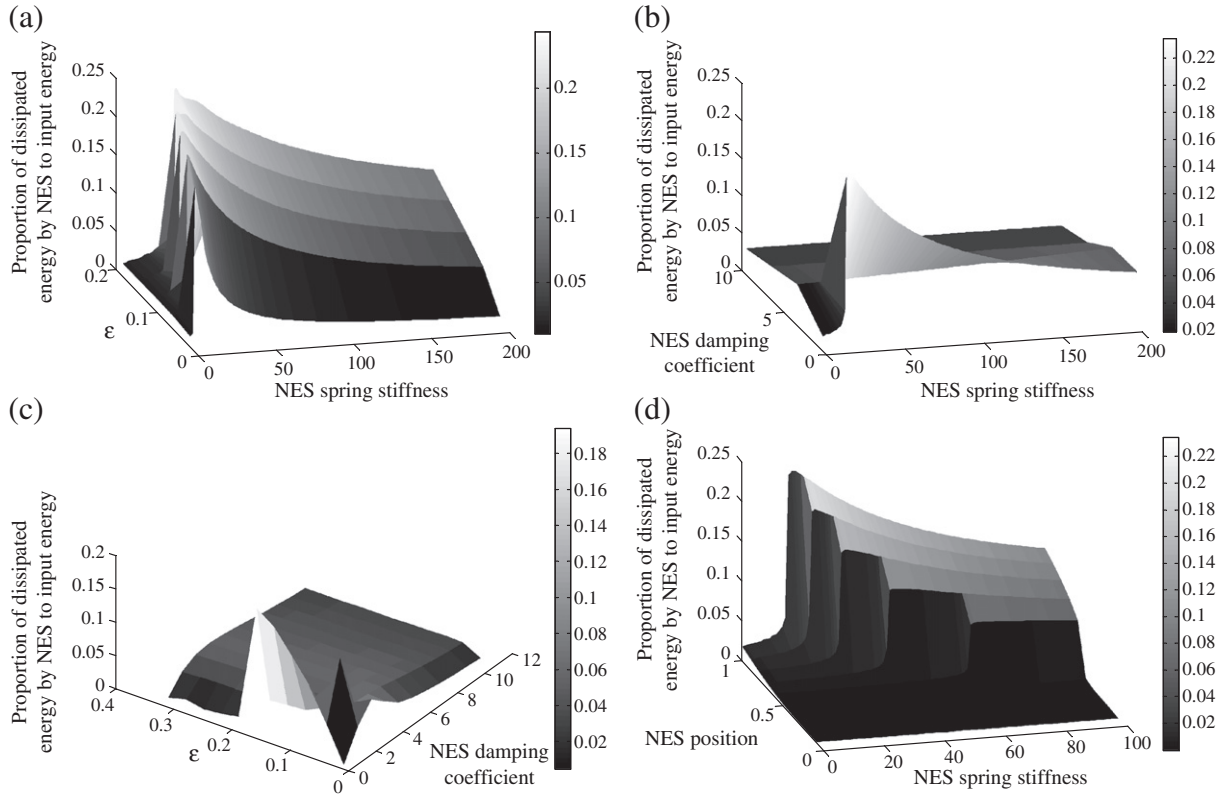

Fig. 6. Contour plots of input energy dissipated by the NES as a function of: (a) ε and the NES spring stiffness, (b) the NES spring stiffness and the NES damping coefficient, (c) ε and the NES damping coefficient, (d) the NES spring stiffness and the NES position.

Table 2
Optimal parameter values for cantilever beam and NES.

Beam				NES#1				NES#2		
$\bar{B}$	$\bar{\beta}$	T	$\frac{\bar{s}}{\bar{L}}$	ε	$\bar{C}$	$\bar{k}_1$	$\bar{k}$	ε	$\bar{C}$	$\bar{k}$
11	0.5	0.3	1	0.1	0.5	1	17	0.1	0.5	13

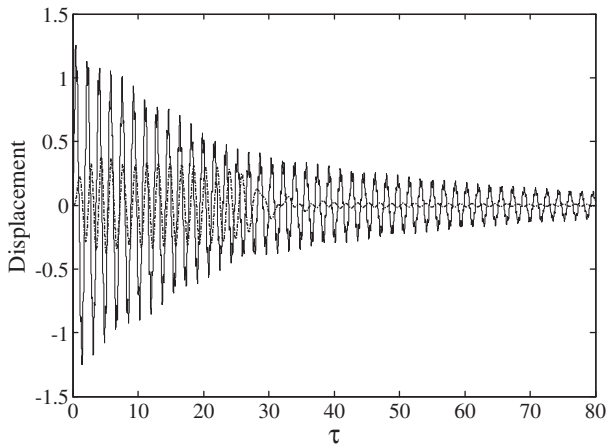

Fig. 7. Transient response of NES#1 for $\bar{B} = 11$. Dash-dot line: NES displacement; solid line: beam displacement.

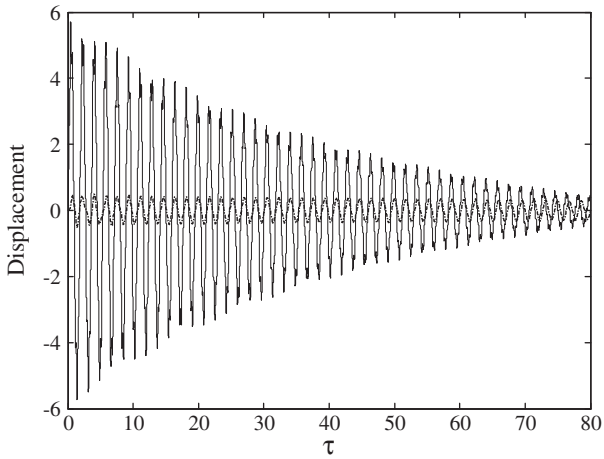

Fig. 8. Transient response of NES#1 for $\bar{B} = 50$. Dash-dot line: NES displacement; solid line: beam displacement.

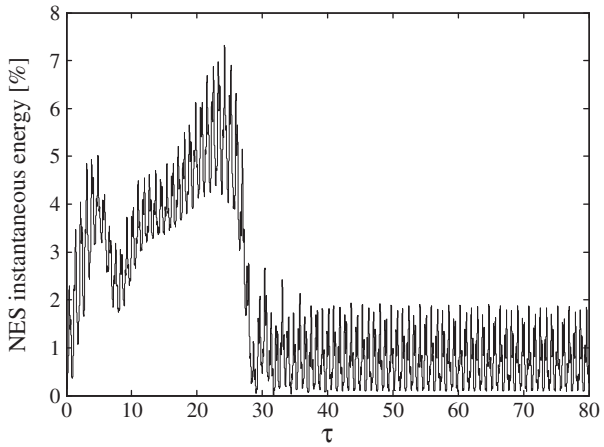

Fig. 9. Instantaneous total energy in the NES of NES#1 for $\bar{B} = 11$.

bifurcations and topological structure of NNMs of the ungrounded system are studied. It is assumed that internal resonances just occur between the nonlinear attachment and the linearized modes of the beam, i.e. internal resonances between the linear modes of the beam are not taken into account. First, examining the NNMs at frequencies in the vicinity of the zero linear frequency, and

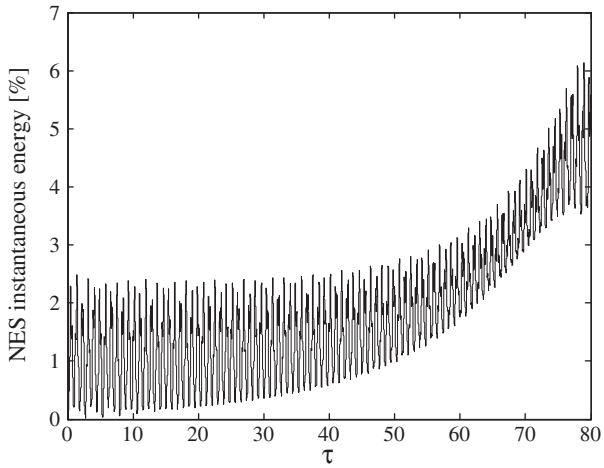

Fig. 10. Instantaneous total energy in the NES of NES#1 for $\bar{B} = 50$.

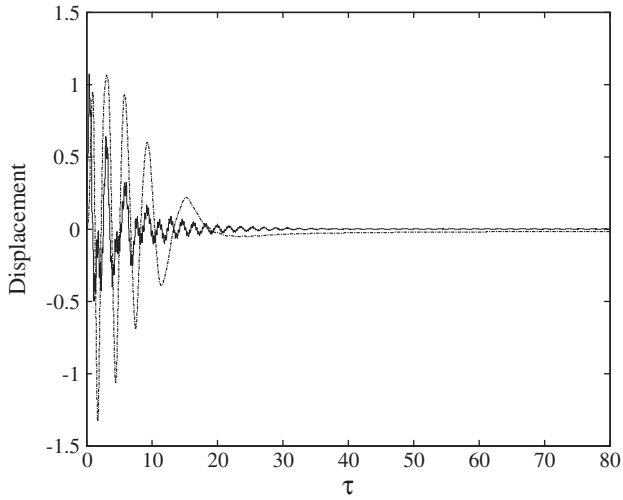

Fig. 11. Transient response of NES#2. Dash-dot line: NES displacement; solid line: beam displacement.

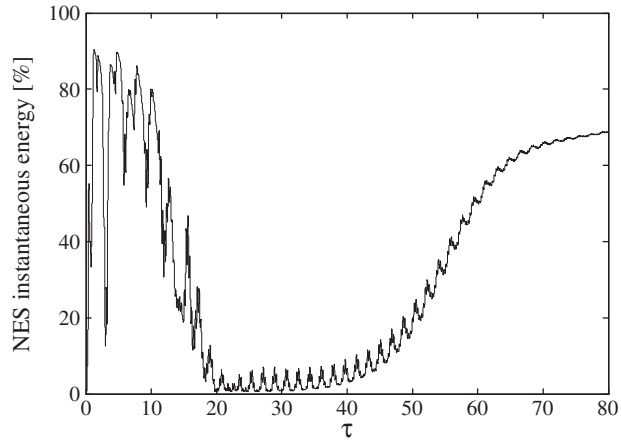

Fig. 12. Instantaneous total energy in the NES of NES#2.

then, the NNMs at frequencies close to higher linear frequencies will be studied. Hence, the equations of motion of the undamped and unforced system can be expressed as follows:

$$\begin{aligned}
&\varepsilon\ddot{w}(t)+\varepsilon K\left[w(t)-q_0(t)\Phi_0(d)-\textstyle\sum_{r=1}^{N}q_r(t)\Phi_r(d)\right]^3=0\\
&\ddot{q}_0(t)+\varrho_0 q_0(t)+\left\{\varepsilon K\left[q_0(t)\Phi_0(d)+\textstyle\sum_{r=1}^{N}q_r(t)\Phi_r(d)-w(t)\right]^3\right\}\Phi_0(d)=0\\
&\ddot{q}_h(t)+\varrho_h q_h(t)+\left\{\varepsilon K\left[\textstyle\sum_{r=0}^{N}q_r(t)\Phi_r(d)-w(t)\right]^3\right\}\Phi_h(d)=0\quad ,h=1,\ldots,N
\end{aligned}\tag{10}$$

where:

$$\varrho_h=\frac{b_{sh}}{b_{fh}},\quad K=\frac{k}{b_{fh}}\simeq k,\quad M=1\,,\quad EI=1,\quad \varepsilon=0.1,\quad d=L.$$

As mentioned earlier and according to Eq. (10), the influential parameters on TET realization in the system are just ε, the NES position and spring stiffness.

Complex variables can be introduced in the following form:

$$\begin{aligned}
&\chi_v = \dot{v} + i\omega_0 v \\
&\chi_0 = \dot{q}_0 + i\omega_0 q_0 \\
&\chi_r = \dot{q}_r + i\omega_r q_r \ , \quad r = 1,\ldots,N \\
&v = \frac{\chi_v - \bar{\chi}_v}{2i\omega_0}, \quad \ddot{v} = \dot{\chi}_v - \frac{i\omega_0}{2}(\chi_v + \bar{\chi}_v)
\end{aligned} \tag{11}$$

where subscript bar denotes complex conjugate.

Replacing the preceding relation in Eq. (10), one may have:

$$\begin{aligned}
&\varepsilon\left[\dot{\chi}_v - \frac{i\omega_0}{2}(\chi_v + \bar{\chi}_v)\right] + \varepsilon K\left[\frac{\chi_v - \bar{\chi}_v}{2i\omega_0} - \frac{\chi_0 - \bar{\chi}_0}{2i\omega_0}\Phi_0(d) - \sum_{r=1}^{N}\frac{\chi_r - \bar{\chi}_r}{2i\omega_r}\Phi_r(d)\right]^3 = 0 \\
&\dot{\chi}_0 - \frac{i\omega_0}{2}(\chi_0 + \bar{\chi}_0) + \varrho_0\frac{\chi_0 - \bar{\chi}_0}{2i\omega_0} + \left\{\varepsilon K\left[\frac{\chi_0 - \bar{\chi}_0}{2i\omega_0}\Phi_0(d) + \sum_{r=1}^{N}\frac{\chi_r - \bar{\chi}_r}{2i\omega_r}\Phi_r(d) - \frac{\chi_v - \bar{\chi}_v}{2i\omega_0}\right]^3\right\}\Phi_0(d) = 0 \\
&\dot{\chi}_h - \frac{i\omega_h}{2}(\chi_h + \bar{\chi}_h) + \varrho_h\frac{\chi_h - \bar{\chi}_h}{2i\omega_h} + \left\{\varepsilon K\left[\sum_{r=0}^{N}\frac{\chi_r - \bar{\chi}_r}{2i\omega_r}\Phi_r(d) - \frac{\chi_v - \bar{\chi}_v}{2i\omega_0}\right]^3\right\}\Phi_h(d) = 0, \quad h = 1,\ldots,N
\end{aligned} \tag{12}$$

Here, the complex variables of the former equations will be substituted by variables consisting a slow oscillating term and a fast oscillating term that are given by:

$$\chi_v = \zeta_v e^{i\omega_0 t}, \quad \chi_0 = \zeta_0 e^{i\omega_0 t}, \quad \chi_h = \zeta_h e^{i\omega_h t}, \quad h = 1,\ldots,N. \tag{13}$$

After substituting Eq. (13) into Eq. (12), the resulting equations will be averaged over their fast frequency components using averaging method presented by [18]. The procured equations in terms of slowly-varying components are represented as follows:

$$\begin{aligned}
&\varepsilon\dot{\zeta}_v + \frac{i\varepsilon\omega_0}{2}\zeta_v + i\frac{3K\varepsilon}{8{\omega_0}^3}\left[-\zeta_v|\zeta_v|^2 + \zeta_0|\zeta_0|^2\Phi_0(d)^3 + \zeta_v^2\bar{\zeta}_0\Phi_0(d) + 2|\zeta_v|^2\zeta_0\Phi_0(d) - \zeta_0^2\bar{\zeta}_v\Phi_0(d)^2 - 2|\zeta_0|^2\zeta_v\Phi_0(d)^2\right. \\
&\quad \left. -2{\omega_0}^2\zeta_v\sum_{r=1}^{N}\frac{\Phi_r(d)^2}{\omega_r^2}|\zeta_r|^2 + 2{\omega_0}^2\zeta_0\Phi_0(d)\sum_{r=1}^{N}\frac{\Phi_r(d)^2}{\omega_r^2}|\zeta_r|^2\right] = 0 \\
&\dot{\zeta}_0 + i\frac{\omega_0}{2}\zeta_0 - i\frac{\varrho_0}{2\omega_0}\zeta_0 + i\frac{3K\varepsilon}{8{\omega_0}^3}\left[\zeta_v|\zeta_v|^2\Phi_0(d) - \zeta_0|\zeta_0|^2\Phi_0(d)^4 + \zeta_0^2\bar{\zeta}_v\Phi_0(d)^3 + 2|\zeta_0|^2\zeta_v\Phi_0(d)^3 - \zeta_v^2\bar{\zeta}_0\Phi_0(d)^2 - 2|\zeta_v|^2\zeta_0\Phi_0(d)^2\right. \\
&\quad \left. + 2{\omega_0}^2\zeta_v\Phi_0(d)\sum_{r=1}^{N}\frac{\Phi_r(d)^2}{\omega_r^2}|\zeta_r|^2 - 2{\omega_0}^2\zeta_0\Phi_0(d)^2\sum_{r=1}^{N}\frac{\Phi_r(d)^2}{\omega_r^2}|\zeta_r|^2\right] = 0 \\
&\dot{\zeta}_h + i\left(\frac{\omega_p}{2} - \frac{\varrho_h}{2\omega_h}\right)\zeta_h + i\frac{K\varepsilon}{8{\omega_h}^3}\left[9\zeta_h|\zeta_h|^2\Phi_h(d)^3 - 6\frac{{\omega_h}^2}{\omega_0^2}\zeta_h|\zeta_v|^2\Phi_h(d)^2 - 6\Phi_h(d){\omega_h}^2\zeta_h\sum_{r=0}^{N}\frac{\Phi_r(d)^2}{\omega_r^2}|\zeta_r|^2\right] = 0, \quad h = 1,\ldots,N
\end{aligned} \tag{14}$$

Using polar coordinate system, the slowly varying amplitudes (ζ_j) will be considered in terms of real slowly varying amplitude and phase according to:

$$\zeta_v = A_v e^{i\gamma_v}, \quad \zeta_0 = A_0 e^{i\gamma_0}, \quad \zeta_h = A_h e^{i\gamma_h}, \quad h = 1,\ldots,N. \tag{15}$$

Introducing the above mentioned variables into Eq. (14) and setting the real parts of the obtained equations to zero, the following sets of equations are obtained:

$$\varepsilon\dot{A}_v + \frac{3K\varepsilon}{8{\omega_0}^3}\left\{\left[-A_0^3\Phi_0(d)^3 - A_v^2A_0\Phi_0(d) - 2{\omega_0}^2A_0\Phi_0(d)\sum_{r=1}^{N}\frac{\Phi_r(d)^2}{\omega_r^2}{A_r}^2\right]\sin(\gamma_0 - \gamma_v) + A_0^2A_v\Phi_0(d)^2\sin(2\gamma_0 - 2\gamma_v)\right\} = 0 \tag{16a}$$

$$\dot{A}_0 + \frac{3K\varepsilon}{8{\omega_0}^3}\left\{\left[A_v^3\Phi_0(d) + A_0^2A_v\Phi_0(d)^3 + 2{\omega_0}^2A_v\Phi_0(d)\sum_{r=1}^{N}\frac{\Phi_r(d)^2}{\omega_r^2}{A_r}^2\right]\sin(\gamma_0 - \gamma_v) - A_v^2A_0\Phi_0(d)^2\sin(2\gamma_0 - 2\gamma_v)\right\} = 0 \tag{16b}$$

$$\dot{A}_h = 0 \rightarrow A_h = constant, \quad h = 1,\ldots,N.$$

A_h, $h = 1,\ldots,N$ are the amplitudes of the non-resonant modes, and since, the motion is governed by the zero linear mode, they can be taken zero in further analysis.

From Eqs. (16a) and (16b), one may obtain:

$$\varepsilon A_v^2 + A_0^2 = \eta^2 \tag{17}$$

Also, by setting the imaginary parts to zero, the additional sets of equations are given by:

$$\dot{\gamma}_v = -\frac{\omega_0}{2} + \frac{3K}{8{\omega_0}^3}\left\{A_v^2 + 2A_0^2\Phi_0(d)^2 + \left[-\frac{A_0^3}{A_v}\Phi_0(d)^3 - 3A_vA_0\Phi_0(d)\right]\cos(\gamma_0-\gamma_v) + A_0^2\Phi_0(d)^2\cos(2\gamma_0-2\gamma_v)\right\} = 0 \tag{18a}$$

$$\dot{\gamma}_0 = -\frac{\omega_0}{2} + \frac{\varrho_0}{2\omega_0} + \frac{3K\varepsilon}{8{\omega_0}^3}\left\{-A_0^2\Phi_0(d)^4 + 2A_v^2\Phi_0(d)^2 + \left[-\frac{A_v^3}{A_0}\Phi_0(d) - 3A_vA_0\Phi_0(d)^3\right]\cos(\gamma_0-\gamma_v) + A_v^2\Phi_0(d)^2\cos(2\gamma_0-2\gamma_v)\right\} \tag{18b}$$

$$\dot{\gamma}_h = \underbrace{-\frac{\omega_h}{2} + \frac{\varrho_h}{2\omega_h}}_{0(\varepsilon)} + \underbrace{\frac{3K\varepsilon}{4{\omega_0}^2\omega_h}\left[A_0^2\Phi_0(d)^2\Phi_h(d) + A_v^2\Phi_h(d)^2\right]}_{0(\varepsilon)} \tag{18c}$$

Since all terms in the right hand side of Eq. (18c) are of order ε, one may conclude that the approximate frequency of the non-resonant modes can be expressed as:

$$\Omega_h \approx \omega_h + \left\{-\frac{\omega_h}{2} + \frac{\varrho_h}{2\omega_h} + \frac{3K\varepsilon}{4{\omega_0}^2\omega_h}\left[A_0^2\Phi_0(d)^2\Phi_h(d) + A_v^2\Phi_h(d)^2\right]\right\}, \quad h = 1, \ldots, N.$$

Subtracting Eq. (18b) from Eq. (18a) and setting $\theta = \gamma_0 - \gamma_v$, the equations of motion can be written as:

$$\begin{aligned}\dot{\theta} &- \frac{\varrho_0}{2\omega_0} + \frac{3K\varepsilon}{8{\omega_0}^3}\left\{A_0^2\Phi_0(d)^4 - 2A_v^2\Phi_0(d)^2 + \left[\frac{A_v^3}{A_0}\Phi_0(d) + 3A_vA_0\Phi_0(d)^3\right]\cos(\gamma_0-\gamma_v) - A_v^2\Phi_0(d)^2\cos(2\gamma_0-2\gamma_v)\right\} \\ &+ \frac{3K}{8{\omega_0}^3}\left\{A_v^2 + 2A_0^2\Phi_0(d)^2 + \left[-\frac{A_0^3}{A_v}\Phi_0(d)^3 - 3A_vA_0\Phi_0(d)\right]\cos(\gamma_0-\gamma_v) + A_0^2\Phi_0(d)^2\cos(2\gamma_0-2\gamma_v)\right\} = 0\end{aligned} \tag{19}$$

If $\dot{\theta}, \dot{A}_v$ and $\dot{A}_0$ in Eqs. (16a), (16b) and (19) are set to zero, one has:

$$A_v^2 = \frac{1}{\varepsilon}\left(\eta^2 - A_0^2\right) \tag{20a}$$

$$\begin{aligned}\gamma_0 = \gamma_v &- \frac{\varrho_0}{2\omega_0} + \frac{3K\varepsilon}{8{\omega_0}^3}\left[A_0^2\Phi_0(d)^4 - 2A_v^2\Phi_0(d)^2 + \frac{A_v^3}{A_0}\Phi_0(d) + 3A_vA_0\Phi_0(d)^3 - A_v^2\Phi_0(d)^2\right] \\ &+ \frac{3K}{8{\omega_0}^3}\left[A_v^2 + 2A_0^2\Phi_0(d)^2 + -\frac{A_0^3}{A_v}\Phi_0(d)^3 - 3A_vA_0\Phi_0(d) + A_0^2\Phi_0(d)^2\right] = 0.\end{aligned} \tag{20b}$$

As it can be realized from Eq. (20a), η is a constant and can be considered as an energy-like quantity which shows energy conservation in the system. Solving Eqs. (20a) and (20b) will give the amplitude of the nonlinear attachment A_v and the amplitude of the zero linear mode of the beam A_0. Also, using Eqs. (11), (13) and (15), the following relation will be obtained:

$$w(t) = \frac{A_v}{\omega_0}\sin\left[\omega_0 t + \gamma_v(t) + o\left(\varepsilon^2\right)\right] + o(\varepsilon).$$

Therefore, the frequency of the system composed of the nonlinear attachment, and the cantilever beam when the NNMs are vibrating, can be estimated as:

$$\Omega_0 \approx \omega_0 + \dot{\gamma}_v = \omega_0 + \dot{\gamma_0} = \omega_0 - \frac{\omega_0}{2} + \frac{\varrho_0}{2\omega_0} + \frac{3K\varepsilon}{8{\omega_0}^3}\left[-A_0^2\Phi_0(d)^4 + 2A_v^2\Phi_0(d)^2 - \frac{A_v^3}{A_0}\Phi_0(d) - 3A_vA_0\Phi_0(d)^3 + A_v^2\Phi_0(d)^2\right] \tag{21}$$

It is clearly observable that $\dot{\gamma}_0$ is of order ε and this makes Ω_0 close to ω_0 which is in agreement with the primary assumption of evaluating the NNMs at frequencies close to the zero linear frequency. Moreover, NNMs in the vicinity of the first and second linear modes are computed using the same procedure in order to find more details on the dynamics of energy pumping in higher linear frequencies.

Since, appearance and continuation of the NNMs and so energy pumping completely rely on the conserved energy of the NNMs, this energy in the neighborhood of each linear mode will be computed in the following form:

$$E_i = \frac{\varrho_i A_{0i}^2}{2} + \frac{K}{4}\left[A_{vi} - A_{0i}\Phi_i(d)\right]^4 \quad i = 0, .., N. \tag{22}$$

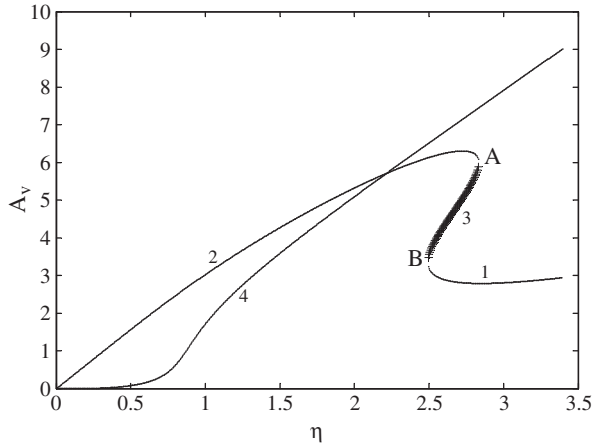

Fig. 13. Amplitude A_v of NES#2 for NNMs close to zero linear mode. ++: unstable NNMs.

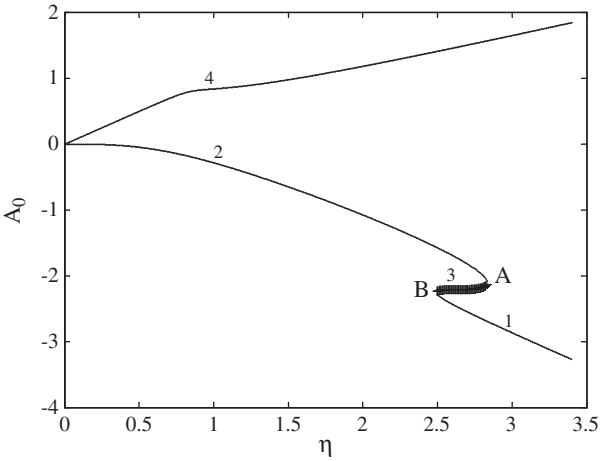

Fig. 14. Amplitude A_0 of NES#2 for NNMs close to zero linear mode. ++: unstable NNMs.

Here, A_{0i} and A_{vi} are the amplitude of the nonlinear attachment, and the amplitude of each linear mode in the vicinity of each linear mode, respectively. Figs. 13–15 depict A_v, A_0 and Ω_0 for NNMs close to the zero linear mode. Regarding NNM 1, it is demonstrated that oscillations of the zero linear mode are comparatively large relative to that of the nonlinear

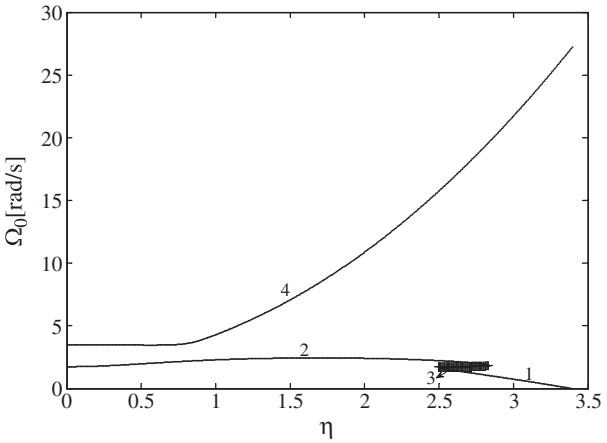

Fig. 15. Frequency Ω_0 of NES#2 for NNMs close to zero linear mode. ++: unstable NNMs.

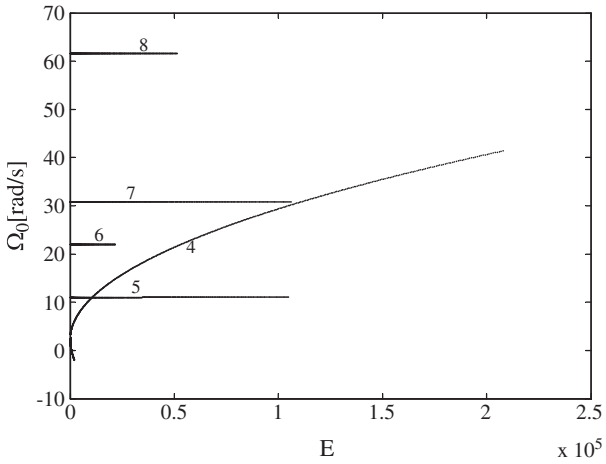

Fig. 16. Frequency Ω_0 of NES#2 for NNMs close to the lowest and higher linear modes versus conserved energy E.

attachment, but mediocre movements of the attachment show the localized motion at the attachment for this branch. Despite of having small movements of the attachment at relatively low amount of η for NNM 4, the attachment will experience a quite large motion for η 0.8. So, the motion associated with this NNM, is localized at the attachment. Also, the motions corresponding to NNMs 2, 3, 5 and 7 are localized at the attachment whereas the ones related to NNMs 6 and 8 are localized at the beam.

Figs. 16 and 17 indicate the NNMs based on the conserved energy and frequency. As it is seen, with increasing energy, NNM 2 and NNM 3 are omitted at saddle bifurcation points A and B, respectively. Also, NNM 1 comes into existence at bifurcation point B. So, only NNM 1 and NNM 4 remain continuous with increasing energy. It is confirmed that at adequately high initial energy, energy pumping can occur through NNM 1 or NNM 4. Indeed, provided that the in-phase linear mode is excited at adequately high energy, the motion will be governed by NNM 1 and energy transfers from the beam to the NES. But if the out-of-phase linear mode is excited at adequately high energy, NNM 4 will be the cause for energy pumping, and since NNM 4 remains continuous with decreasing energy, no jump will take place from this NNM to NNMs 2 or 1 as energy decreases. Provided that both in-phase and out-of-phase linear modes are excited at adequately high energy, resonance capture cascade will occur. Further observations show that the topological structures of NNMs close to the zero linear mode differ from that of NNMs in the neighborhood of the higher linear modes (which have similar structures). Additionally, NNMs close to the lower linear modes will vanish at relatively much lower energy values than the ones close to the higher linear modes. It is worth mentioning that there are no unstable NNMs in the vicinity of the higher linear modes.

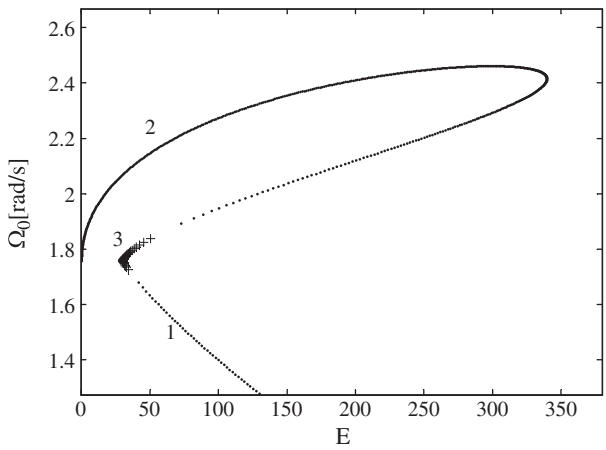

Fig. 17. Close-up of Frequency Ω_0 of NES#2 for NNMs close to the lowest and higher linear modes versus conserved energy E. ++: unstable NNMs.

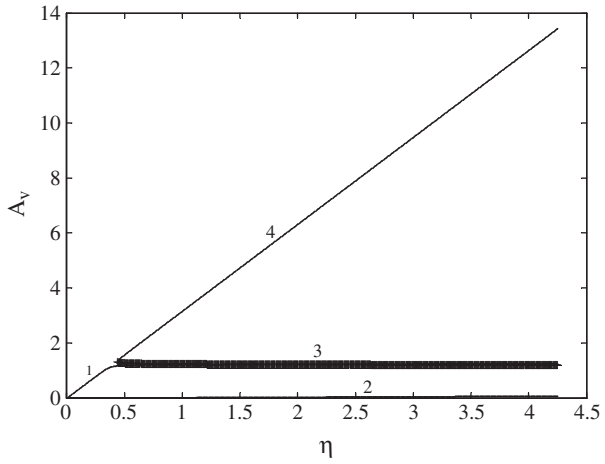

Fig. 18. Amplitude A_v of NES#1 for NNMs close to zero linear mode. ++: unstable NNMs.

3.2. NES#1

In this stage, the previously mentioned procedure will be applied in order to find the NNMs of NES#1. The results can be expressed in the following form:

$$\Omega_0 \approx \omega_0 + \dot{\gamma}_v = \omega_0 + \dot{\gamma_0} = \omega_0 - \frac{\omega_0}{2} + \frac{\varrho_0}{2\omega_0} + \frac{\varepsilon}{2\omega_0}\left[\Phi_0(d)^2 - \frac{A_v}{A_0}\Phi_0(d)\right]$$
$$E_i = \frac{\varrho_i A_{0i}^2}{2} + \frac{K}{4}{A_{vi}}^4 \quad i = 0, ..., N. \tag{23}$$

According to Figs. 18–20, similar to NES#2, there are localized motions at the attachment for NNMs 1, 4, 5 and 7. But for NNMs 2, 6 and 8, the motions related to the beam are relatively large in comparison to the attachment movements. Associated movements to NNM 3 follow a similar manner. Additional details can be obtained by observing the curve corresponding to the conserved energy (see Figs. 21–22). Accordingly, NNMs 3 and 4 are created at bifurcation point A. Contrary to NES#2, NNM 1 will be eliminated almost at low energy level along with NNMs 2 and 3, and there is no bifurcation point at the ending point. So, if the in-phase linear mode is excited at an adequately high energy, there will be no NNM to govern the response. But if the out-of-phase linear mode is excited at an adequately high energy, the response is governed by NNM 4, but with decreasing energy there may be a jump to NNMs 1 or 2 due to the existence of the discontinuity. Consequently, the absence of a continuous NNM in case of excitation of the in-phase linear mode could be the reason for having no significant energy pumping to the NES.

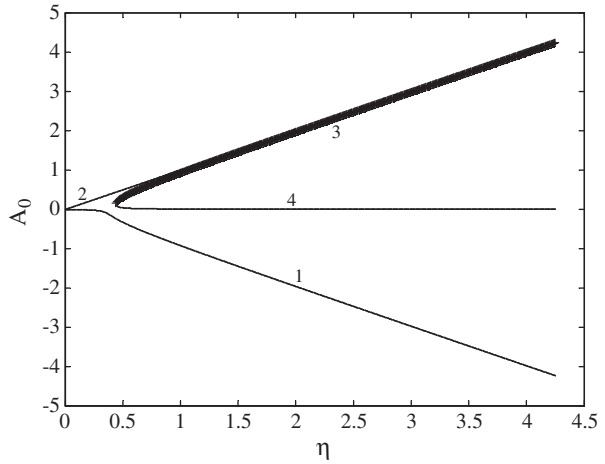

Fig. 19. Amplitude A_0 of NES#1 for NNMs close to zero linear mode. ++: unstable NNMs.

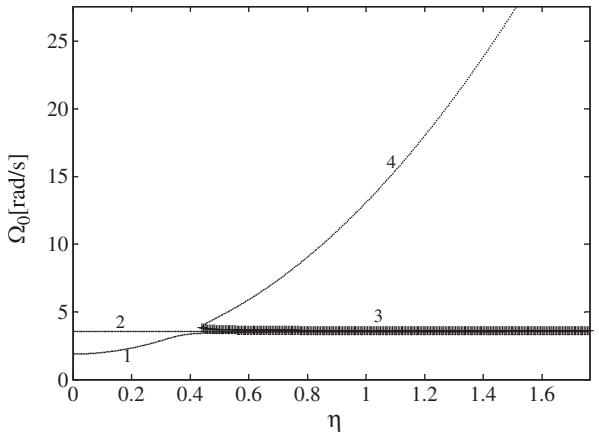

Fig. 20. Frequency Ω_0 of NES#1 for NNMs close to zero linear mode. ++: unstable NNMs.

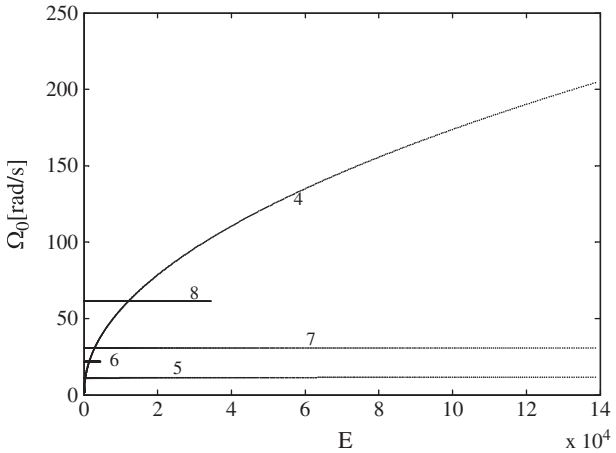

Fig. 21. Frequency Ω_0 of NES#1 for NNMs close to the lowest and higher linear modes versus conserved energy E.

The structures of NNMs close to the higher linear modes highly resemble that of NES#1. In this way, they end at relatively much higher energy values than the ones close to the zero linear mode. Their structures are completely different from that of NNMs close to the zero linear mode, and they are all stable.

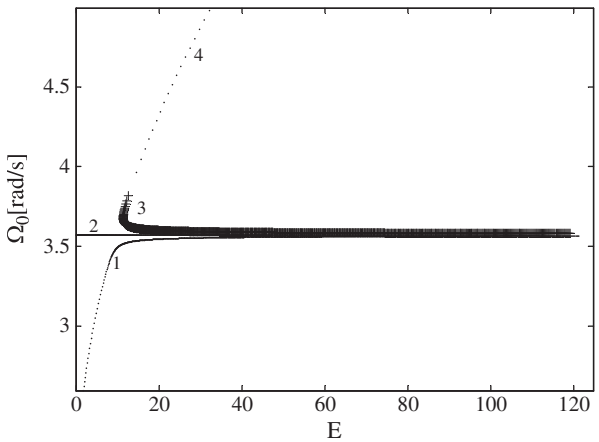

Fig. 22. Close-up of Frequency Ω_0 of NES#1 for NNMs close to the lowest and higher linear modes versus conserved energy E. ++: unstable NNMs.

4. Concluding remarks

NNMs of an undamped and unforced system are very crucial in identifying the conditions for TET realization of the damped system. So, the bifurcations and topological structures of NNMs corresponding to a cantilever beam with two NES configurations (grounded and ungrounded) have been studied in this work. The results indicate that the NNMs corresponding to the ungrounded configuration are relatively different from that of the grounded configuration. It is also demonstrated that energy pumping occurs effectively in an ungrounded configuration which results in about 89% energy dissipation. By contrast, due to lack of a continuous NNM in case of excitation of the in-phase linear mode of the grounded system, there will be no remarkable energy transfer to the NES in this case. This consequence has been also achieved by studying dissipated and instantaneous energies of the system, and thus, the importance of NNMs structures in occurrence of a one-way irreversible energy pumping has been proven for continuous systems in this paper.

References

[1] O.V. Gendelman, Transition of energy to nonlinear localized mode in highly asymmetric system of nonlinear oscillators, Nonlinear Dynamics 25 (2001) 237–253.
[2] A.F. Vakakis, Inducing passive nonlinear energy sinks in linear vibrating systems, Journal of Vibration and Acoustics 123 (3) (2001) 324–332.
[3] O.V. Gendelman, A.F. Vakakis, L.I. Manevitch, R. McCloskey, Energy pumping in nonlinear mechanical oscillators I: dynamics of the underlying Hamiltonian system, Journal of Applied Mechanics 68 (1) (2001) 34–41.
[4] A.F. Vakakis, O.V. Gendelman, Energy pumping in nonlinear mechanical oscillators II: resonance capture, Journal of Applied Mechanics 68 (1) (2001) 42–48.
[5] O.V. Gendelman, D.V. Gorlov, L.I. Manevitch, A.I. Musienko, Dynamics of coupled linear and essentially nonlinear oscillators with substantially different masses, Journal of Sound and Vibration 286 (2005) 1–19.
[6] O.V. Gendelman, C.H. Lamarque, Dynamics of linear oscillator coupled to strongly nonlinear attachment with multiple states of equilibrium, Chaos, Solitons & Fractals 24 (2005) 501–509.
[7] O.V. Gendelman, E. Gourdon, C.H. Lamarque, Quasiperiodic energy pumping in coupled oscillators under periodic forcing, Journal of Sound and Vibration 294 (2006) 651–662.
[8] O.V. Gendelman, Y. Starosvetsky, Quasiperiodic response regimes of linear oscillator coupled to nonlinear energy sink under periodic forcing, Journal of Applied Mechanics 74 (2007) 325–331.
[9] O.V. Gendeman, Y. Starosvetsky, M. Feldman, Attractors of harmonically forced linear oscillator with attached nonlinear energy sink I: description of response regimes, Nonlinear Dynamics 51 (2008) 31–46.
[10] Y. Starosvetsky, O.V. Gendelman, Attractors of harmonically forced linear oscillator with attached nonlinear energy sink II: optimization of a nonlinear vibration absorber, Nonlinear Dynamics 51 (2008) 47–57.
[11] Y. Starosvetsky, O.V. Gendelman, Strongly modulated response in forced 2dof oscillatory system with essential mass and potential asymmetry, Physica D: Nonlinear Phenomena 237 (2008) 1719–1733.
[12] Y. Starosvetsky, O.V. Gendelman, Response regimes of linear oscillator coupled to nonlinear energy sink with harmonic forcing and frequency detuning, Journal of Sound and Vibration 315 (2008) 746–765.
[13] T.P. Sapsis, A.F. Vakakis, O.V. Gendelman, L.A. Bergman, G. Kerschen, D.D. Quinn, Efficiency of targeted energy transfers in coupled nonlinear oscillators associated with 1:1 resonance captures: part II, analytical study, Journal of Sound and Vibration 325 (2009) 297–320.
[14] Young S. Lee, Alexander F. Vakakis, Lawrence A. Bergman, D. Michael McFarland, Suppression of limit cycle oscillations in the van der Pol oscillator by means of passive non-linear energy sinks, Structural Control and Health Monitoring 13 (2006) 41–75.
[15] O.V. Gendelman, T. Bar, Bifurcations of self-excitation regimes in a Van der Pol oscillator with a nonlinear energy sink, Physica D: Nonlinear Phenomena 239 (2010) 220–229.
[16] F. Georgiades, A.F. Vakakis, Dynamics of a linear beam with an attached local nonlinear energy sink, Communications in Nonlinear Science and Numerical Simulation 12 (2007) 643–651.
[17] A.F. Vakakis, L.I. Manevitch, O. Gendelman, L. Bergman, Dynamics of linear discrete systems connected to local, essentially non-linear attachments, Journal of Sound and Vibration 264 (2003) 559–577.
[18] L.I. Manevitch, Description of localized normal modes in the chain of nonlinear coupled oscillators using complex variables, Nonlinear Dynamics 25 (2001) 95–109.